unit cell containing four molecules with carbon atoms located on the face-centered positions. The molecular axes point in the body-diagonal directions as a result of strong quadrupole-quadrupole interactions between the molecules (*18*). Raman and infrared measurements have revealed that the symmetric stretch and the overtone of the bending vibrational states are located in a postresonant region at atmospheric pressure (*19*, *20*). Hence, application of pressure pushes the partly coupled vibrational states further off-resonance. An exact resonance is predicted to occur at a virtual negative pressure of about -5 GPa, where roughly estimated values of 50 and 105 cm^{-1} were obtained for W and δ, respectively. These values are very close to those of ice VII obtained in the present experiment. This agreement seems to be coincidental, rather than a common tendency in triatomic molecules. The chemical bonds of H_2O and CO_2 are too different to permit the extraction of a general tendency for Fermi resonance in molecular solids.

REFERENCES AND NOTES

1. For instance, see R. J. Hemley, L. C. Chen, H. K. Mao, *Nature* **338**, 638 (1989).
2. W. F. Kuhs, J. L. Finney, C. Vettier, D. V. Bliss, *J. Chem. Phys.* **81**, 3612 (1984).
3. J. D. Jorgensen and T. G. Worlton, *ibid.* **83**, 329 (1985).
4. J. D. Jorgensen *et al.*, *ibid.* **81**, 3211 (1984).
5. Ph. Pruzan *et al.*, *ibid.* **97**, 718 (1992).
6. G. E. Walrafen *et al.*, *ibid.* **77**, 2166 (1982).
7. K. R. Hirsch and W. B. Holzapfel, *ibid.* **84**, 2771 (1986).
8. D. D. Klug and E. Whalley, *ibid.* **81**, 1220 (1984).
9. R. G. Munro, S. Block, F. A. Mauer, G. Piermarini, *J. Appl. Phys.* **53**, 6174 (1982). They used the earlier linear ruby-pressure scale in their x-ray diffraction measurement, which tends to underestimate the pressure, for instance, by 1 GPa at 25 GPa. We have corrected their pressures using the nonlinear ruby-pressure scale given in (*16*).
10. R. J. Hemley *et al.*, *Nature* **330**, 737 (1987).
11. R. J. Nelmes *et al.*, *Phys. Rev. Lett.* **71**, 1192 (1993).
12. H. Shimizu, M. Ohnishi, S. Sasaki, Y. Ishibashi, *ibid.* **74**, 2820 (1995).
13. F. Rasetti, *Nature* **123**, 205 (1929).
14. E. Fermi, *Z. Phys.* **71**, 250 (1931).
15. K. Aoki *et al.*, *Jpn. J. Appl. Phys.* **26**, 2107 (1987).
16. H. K. Mao *et al.*, *J. Appl. Phys.* **49**, 3276 (1978).
17. W. Schindler, T. W. Zerda, J. Jonas, *J. Chem. Phys.* **81**, 4306 (1984).
18. W. H. Keesom and J. W. L. Kohler, *Physica* **1**, 167 (1934).
19. R. C. Hanson and L. H. Jones, *J. Chem. Phys.* **75**, 102 (1981).
20. H. Olijnyk *et al.*, *ibid.* **88**, 4204 (1988).

22 September 1994; accepted 8 March 1995

Mesostructure Design with Gemini Surfactants: Supercage Formation in a Three-Dimensional Hexagonal Array

Qisheng Huo, Rosa Leon, Pierre M. Petroff, Galen D. Stucky*

At low temperatures, liquid crystal–like arrays made up of inorganic-cluster and organic molecular units readily undergo reversible lyotropic transformations. Gemini surfactants, with two quaternary ammonium head groups separated by a methylene chain of variable length and with each head group attached to a hydrophobic tail, can be used to control organic charge sitting relative to the bivariable hydrophobic tail configurations. This approach has led to the synthesis of a mesophase (SBA-2) that has three-dimensional hexagonal ($P6_3/mmc$) symmetry, regular supercages that can be dimensionally tailored, and a large inner surface area. This mesostructure analog of a zeolite cage structure does not appear to have a lyotropic surfactant or lipid liquid crystal mesophase counterpart. Through the modification of gemini charge separation and each of the two organic tails, these syntheses can be used to optimize templating effects, including the synthesis of MCM-48 at room temperature.

Ordered silicate mesoporous molecular sieves have been synthesized (*1*– *5*) by the organization of organic molecules with inorganic molecular species. Low-temperature synthesis methods and kinetic control can be used to uncouple inorganic polymerization from the initial cooperative assembly of inorganic cluster ions and surfactant ions into liquid crystal–like arrays (*4*–*6*). These liquid crystal–like phases are similar to conventional surfactant and lipid lyotropic liquid crystal arrays. However, they cannot be adequately described by thermodynamic and modeling descriptions that only implicitly include polycharged cluster anions as part of the charged bilayer. The multidentate anions have large formation constants with the surfactant cations, have low solubilities, and structurally direct the arrangement of the organic surfactants through both the number of anionic sites that are present (generally determined by pH) and the orientation of the organic surfactant with respect to the molecular inorganic surface (*7*). These characteristics strongly suggest that new lyotropic liquid crystal phases and behavior might be obtained in biphase inorganic-organic mesostructure synthesis. Because of the saltlike character of the product phases and the ability to polymerize the inorganic or organic phase into periodic long-range structures, the mesocomposite materials can be used to study lyotropic liquid crystal–like arrangements in more detail (*6*).

The relative positions and distances of head groups of conventional mono(quaternary ammonium) surfactants are determined mainly by electrostatic interactions, and also by the packing requirements of the disordered alkyl chains. By coupling the head groups with a molecular spacer, one can control the distance between the head groups, that is, the value of a_0, the effective head group area (*8*). Oligomeric or polymeric charged surfactants with a spatially separated charge center can either act as a chelating group to a given cluster surface or serve to orient clusters with respect to each other. By this means, we can change the packing parameter g (*8*) of the surfactant–inorganic cluster unit with polycharged surfactants. In this report, we describe recent mesoporous material synthesis results obtained with gemini surfactants (*9*), $C_nH_{2n+1}N^+(CH_3)_2(CH_2)_sN^+(CH_3)_2$-$C_mH_{2m+1}$ (designated as $C_{n\text{-}s\text{-}m}$), and silica. The mesoporous structure can be considerably modified by changing the length and nature of both the side chain and the spacer group. The end member of this family, $C_{n\text{-}s\text{-}1}$, gives a particularly interesting three-dimensional (3D) hexagonal cage structure (SBA-2). Cage-structured mesoporous solids have possible advantages in catalysis and separation applications. Of the reported mesoporous structures, the M41S molecular sieves, MCM-41 and MCM-48, possess uniform pore channels without cages. The same is true of SBA-3 (acid, pH < 1, synthesized silica phase with an x-ray diffraction pattern similar to that of MCM-41) and cubic phases synthesized in concentrated acid solution (*4*, *5*). For example, the cubic ($Pm\bar{3}n$) silica structure, SBA-1, is synthesized in the presence of surfactants with large head groups (such as, alkyltriethylammonium) in acidic media (*4*). A sample of SBA-1 [cell parameter $a = 79.2$ Å, synthesized with $C_{18}H_{37}N(C_2H_5)_3{}^+$] has a BET (Brunauer-Emmett-Teller) surface area of 1256 m^2 g^{-1}, with a pore diameter of 20

Q. Huo, Department of Chemistry, University of California, Santa Barbara, CA 93106, USA.
R. Leon and P. M. Petroff, QUEST, University of California, Santa Barbara, CA 93106, USA.
G. D. Stucky, Departments of Chemistry and Materials, University of California, Santa Barbara, CA 93106, USA.

*To whom correspondence should be addressed.

Å. The pores are sharply defined and show no hysteresis in the absorption-desorption isotherm (Fig. 1A). An α_s plot (*10*) shows no evidence of micropores. These data suggest a continuous pore structure.

In contrast, SBA-2, is a regular caged mesoporous silicate material. Its analog has not been previously observed in a lyotropic liquid crystal system. We synthesized it (*11*) using divalent quaternary ammonium surfactants $C_{n\text{-}s\text{-}1}$ (such as $C_{12\text{-}3\text{-}1}$, $C_{16\text{-}2\text{-}1}$, $C_{16\text{-}3\text{-}1}$, $C_{16\text{-}6\text{-}1}$, and $C_{18\text{-}3\text{-}1}$) as templates. Our experimental results imply that SBA-2 possesses the space group $P6_3/mmc$ symmetry (number 194) and is derived from a hexagonal close packing of globular surfactant-silicate arrays (*12*). After calcination, the large cage-structured mesoporous silica framework remains.

The x-ray diffraction (XRD) patterns of SBA-2 (Fig. 2) can be indexed in the space group $P6_3/mmc$ with cell parameter ratios of c/a = 1.61 to 1.63; the ideal c/a ratio for a typical hexagonal close-packed (hcp) phase is 1.633. Several electron diffraction patterns can be indexed in this space group and confirm the space group and lattice parameters (Fig. 3). The transmission electron micrographs in Fig. 3 show a regular array of pores for different orientations.

Solid N_2 (*13*) at 300 K and 2.94 GPa possesses $P6_3/mmc$ symmetry and a c/a ratio of 1.62. However, solid N_2 at 299 K and 4.9 GPa has $Pm\bar{3}n$ symmetry (*14*). It has been suggested that the cubic (I_1) mesophase has the same structure as solid N_2 ($Pm\bar{3}n$) (*15*). The $C_{n\text{-}s\text{-}1}$ surfactants have a high charge density and large head groups, which favors globular micellar aggregates (*16*). For example, $Pm\bar{3}n$ (~33 to 67 weight %) hexagonal and lamellar phases were observed for a $C_{12\text{-}3\text{-}1}Cl$-water system at room temperature (*16*). The surfactant $C_{n\text{-}s\text{-}1}$ gives the $Pm\bar{3}n$ phase in a surfactant-water binary system and the $P6_3/mmc$ silicate mesophase under our synthesis condition. Structural simi-

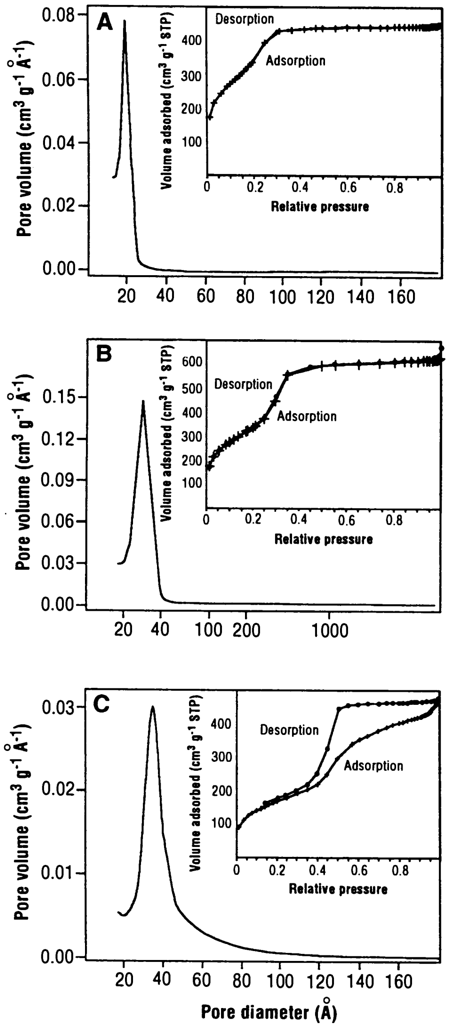

Fig. 1. Pore size distribution (plot of differential volume as a function of pore size) for (**A**) SBA-1, (**B**) SBA-3 [$C_{18}H_{37}N(CH_3)_3^+$ was used as template], and (**C**) SBA-2. (**Insets**) Corresponding N_2 adsorption and desorption isotherm at 77 K, measured with a Micromeritics ASAP 2000 system. The data were analyzed by the BJH (Barrett-Joyner-Halenda) method with the Halsey equation for multilayer thickness. Pressure is measured relative to P_0, the saturation pressure. The pore size distribution curve came from the analysis of the adsorption branch of the isotherm.

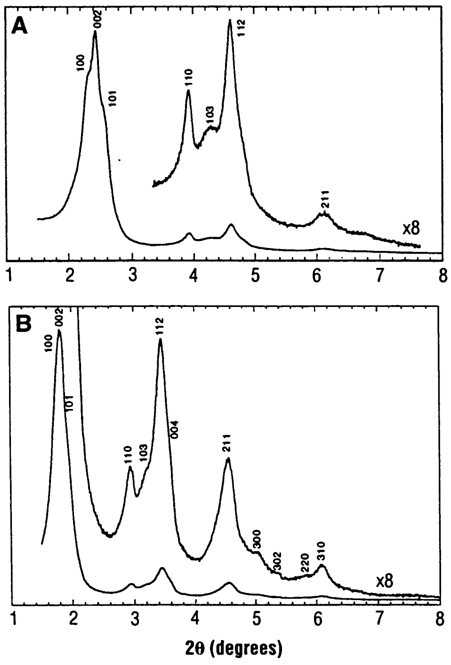

Fig. 2. The x-ray diffraction patterns of SBA-2. The patterns were obtained from a Scintag PAD with Cu Kα radiation. (**A**) Calcined SBA-2. Synthesis conditions: 0.05 M of C_{16-3-1}, 0.5 M of NaOH, 1 M of TEOS, and 150 M of H_2O at room temperature for 2 hours. The template was removed at 500°C for 2 hours. (**B**) As-made SBA-2. Synthesis conditions: 0.05 M of C_{16-3-1}, 0.5 M of NaOH, 0.58 M of TMB, 1 M of TEOS, and 150 M of H_2O at room temperature for 5 hours. A portion of each curve is multiplied (×8) to show detail.

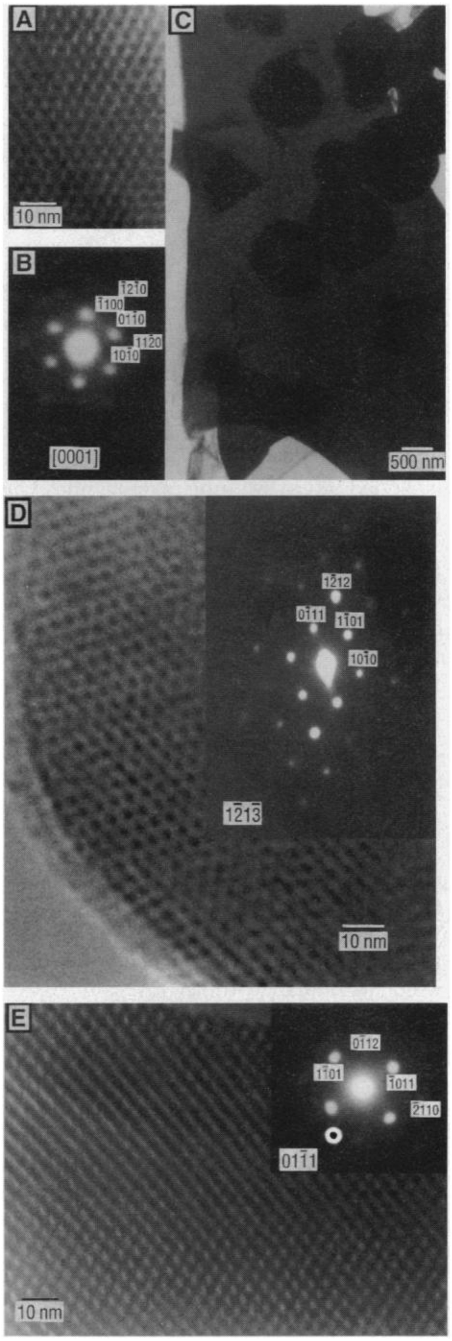

Fig. 3. Transmission electron micrographs for SBA-2 from samples prepared by adhering a large number of crystallites of SBA-2 onto a holey carbon film on a Cu grid. We used 200FX and 2010 JEOL electron microscopes operated at 200 keV. Electron diffraction patterns were obtained at 280-cm camera length. Examples of (**A**) lattice images and (**B**) electron diffraction (ED) patterns of this mesostructure viewed along the [0001] zone axis. (**C**) Scanning electron micrograph. The extended sheet (up to 20 μm) with better morphology and longer range crystallinity than normally obtained for other mesoporous materials. Lattice images along the (**D**) [$1\bar{2}1\bar{3}$] zone axis and (**E**) [$01\bar{1}1$] zone axis. The corresponding ED patterns are shown in the insets. Note the high resolution of the images. The absence of $hh\bar{h}0l$ (l is odd) reflections further confirm the $P6_3/mmc$ space group.

larity between solid N_2 and SBA-2 is consistent with the structure of SBA-2 arising from a close-packed arrangement of organized organic and inorganic arrays.

We have obtained SBA-2 with varying unit cell and cage sizes by using surfactants with different chain lengths over a wide synthesis range (from c = 77 Å for $C_{12\text{-}3\text{-}1}$ to c = 102 Å for $C_{18\text{-}3\text{-}1}$).

Organic cosolvents have been used to control the synthesis of mesoporous solids (*1, 2, 5*) as well as lyotropic mesophases of surfactant-solvent binary systems (*17, 18*) (Fig. 4). Apolar additives, acting as cosolvents, penetrate into the center hydrophobic part of the micelle and swell the micelle size. When trimethylbenzene (TMB) is added as a swelling agent, relatively large changes in the unit cell are observed. This approach was used in large-pore MCM-41 synthesis (*1, 2*). For example, $C_{16\text{-}3\text{-}1}$ yields SBA-2 with a = 62 Å and c = 100 Å when the TMB/tetraethyl orthosilicate (TEOS) concentration ratio is 1.1; without TMB, a cell with a = 54 Å and c = 87 Å was found. A suitable polar additive can enter the hydrophobic-hydrophilic region (first few carbon atoms) of the micelle, with a relative increase in the volume of the hydrophobic core to form surfactant molecule aggregates with a lower curvature surface (from sphere to rod). For example, when *t*-amyl alcohol, a polar additive, was added into the synthesis mixture, the SBA-2 product is replaced by MCM-41, which is similar to the synthesis of SBA-1 with $C_{16}H_{33}N^+(C_2H_5)_3$ as a template without *t*-amyl alcohol and the synthesis of SBA-3 with *t*-amyl alcohol.

The template in SBA-2 can be removed by calcination at high temperature (500° to 600°C). This material is thermally stable up to 800°C. The XRD pattern of calcined SBA-2 at 500°C is shown in Fig. 2. Like MCM-41 and MCM-48, the cell of SBA-2 contracts during calcination (5 to 30 Å). The calcined sample of SBA-2 (a = 63.8 Å and c = 103.4 Å) has a N_2 BET surface area of 609 $m^2\ g^{-1}$, with a narrow distribution of pore diameters at 35 Å. The N_2 isotherm is a type IV isotherm with a H2 hysteresis loop (*19*) (Fig. 1C), in contrast to MCM-41 (*20*) (Fig. 1B). Hysteresis is similarly observed for ~25 Å diameter pores for SBA-2 (a = 47.6 Å and c = 76.4 Å). This result suggests that SBA-2 has bottle-shaped pores or a network of pores (*19*). The N_2 isotherm was analyzed by means of an α_s plot (*10*). The N_2 adsorption data on nonporous hydroxylated silica (*21*) have been used to create the α_s plot as in (*20*). The shape of the α_s plot of SBA-2 appears to confirm that monolayer-multilayer adsorption has occurred on the pore walls before the onset of capillary condensation at relative pressure P/P_0 = 0.40 (P_0 is the saturation pressure). The absence of any detectable micropore filling at low P/P_0 in SBA-2 is confirmed by the fact that the initial linear region of α_s plots can be extrapolated back to the origin.

Formally, the gemini surfactants (*22–24*), $C_{n\text{-}s\text{-}m}$ (n = m), may be considered as a two-chain divalent surfactant. The hydrophilic head group and the polymethylene spacer (C_sH_{2s+1}) are restricted on the surface of the micelle because of the hydrophobic tails at the two ends. The relative changes of a_0 with s are large (*24*), and packing parameter g shows similar large variations. Drastic changes in the characteristics and behavior of the $C_{m\text{-}s\text{-}m}$ micelles and mesophases are consequently expected to occur as s varies. Although g can still be used to express the packing result of the surfactants–molecular inorganic ion pairs in our synthesis systems, additional factors affect its value. In general, their templating parallels their lyotropic liquid crystal behavior in surfactant-water binary systems (*22–24*). Surfactants with small values of s favor the lamellar phase (MCM-50), and those with larger values of s favor the hexagonal phase (MCM-41) (Fig. 5). $C_{12\text{-}12\text{-}12}$ yields MCM-41 at room temperature. Note that aqueous solutions of $C_{12\text{-}12\text{-}12}$ remain micellar over the whole range of concentration and do not form a lyotropic liquid crystal phase (*23*). This circumstance demonstrates the importance of the inorganic species in the cooperative templating mechanism for the concentration region in which the synthesis is carried out.

The use of $C_{16\text{-}12\text{-}16}$ gives MCM-48 at both room temperature and high synthesis temperature(100°C). $C_{16\text{-}12\text{-}16}$ favors the formation of the cubic ($Ia\bar{3}d$) phase, even without the organic additive and with either Cab-O-Sil (SiO_2) or sodium silicate solution as the silica source (*25*). Its micellar structure is similar to the cetyltrimethylammonium bromide–polar additive–water mixture in certain respects (*18*). The spacer ($C_{12}H_{24}$) of $C_{16\text{-}12\text{-}16}$ is long enough to partially penetrate the hydrophobic core of the micelle, but it does not penetrate very deeply because it is bonded to the head groups. This penetration shortens the effective tail length, giving materials with smaller pore size. In the limit of longer tails (>$C_{12}H_{24}$), the gemini surfactant geometry could approach a modified two-tail surfactant configuration.

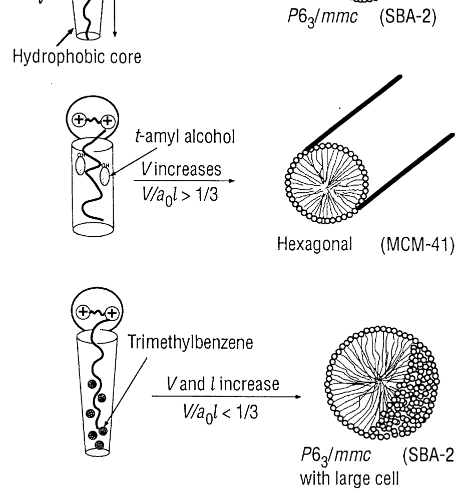

Fig. 4. The effect of organic additives on synthesis product when $C_{n\text{-}s\text{-}1}$ surfactant was used. The silicate species around the head groups of surfactants is not shown, for clarity.

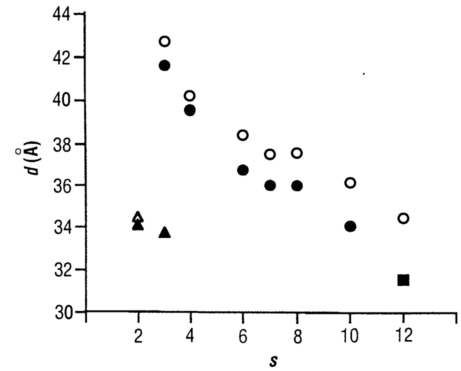

Fig. 5. Typical synthesis results with gemini surfactants, $C_{16\text{-}s\text{-}16}$. The d is d_{100} for MCM-41, SBA-3, and lamellar phase and d_{211} for MCM-48. Symbols: open circles, SBA-3; solid circles, MCM-41 (base); open triangle, lamellar phase (acid); solid triangles, MCM-50 (base); and solid square, MCM-48. Synthesis conditions for acid synthesis: 0.06 M of $C_{16\text{-}s\text{-}16}$, 4.8 M of HCl, 1 M of TEOS, and 130 M of H_2O at room temperature for 1.5 hours; for base synthesis: 0.06 M of $C_{16\text{-}s\text{-}16}$, 0.65 M of NaOH, 1 M of TEOS, and 150 M of H_2O at room temperature for 1 day.

The effect of mixing surfactants can be thought of as simply averaging the two surfactant packing parameters. For example, a mixture of $C_{16\text{-}12\text{-}16}$ and $C_{16\text{-}3\text{-}1}$ was used in silicate mesophase synthesis; the products vary from MCM-48 to SBA-2 through MCM-41 as the fraction of $C_{16\text{-}3\text{-}1}$ increases in the mixture.

In summary, lyotropic liquid crystal mesophase analogs—MCM-41 (hexagonal) (*1, 2*), MCM-48 (cubic $Ia\bar{3}d$) (*1–3*), MCM-50 (lamellar) (*1, 2*), SBA-3 (*4, 5*), and SBA-1 (cubic $Pm\bar{3}n$) (*4, 5*)—and SBA-2, which has no lyotropic mesophase analog, have been synthesized. This suggests that it should be possible to obtain other cage- or channel-structured mesoporous solids by this synthesis method.

REFERENCES AND NOTES

1. C. T. Kresge *et al.*, *Nature* **359**, 710 (1992).
2. J. S. Beck *et al.*, *J. Am. Chem. Soc.* **114**, 10834 (1992).
3. A. Monnier *et al.*, *Science* **261**, 1299 (1993).
4. Q. Huo *et al.*, *Nature* **368**, 317 (1994).
5. Q. Huo *et al*, *Chem. Mater.* **6**, 1176 (1994).
6. A. Firouzi *et al.*, *Science* **267**, 1138 (1995).
7. J. Emmer and M. Wiebcke, *Chem. Commun.* **1994**, 2079 (1994).
8. The description of surfactant organization in amphophilic liquid crystal arrays is described in terms of the local effective surfactant packing parameter $g = V/a_0 l$, where V is the total volume of the surfactant chains plus any cosolvent organic molecules between the chains, a_0 is the effective head group area at the micelle surface, and l is the kinetic surfactant tail length (Fig. 4). Spherical micelles will form if $g < 1/3$, rodlike micelles if $1/3 < g < 1/2$, vesicles or bilayers if $1/2 < g < 1$, and inverted micelles if $g > 1$. For details, see J. N. Israelachvili, D. J. Mitchell, B. W. Ninham, *Faraday Trans. 2* **72**, 1525 (1976).
9. The surfactants were synthesized by reactions of the α,ω-dibromoalkanes with *N,N,N*-alkyldimethylamine or alkanediyl-α,ω-bis(dimethylamine) with a corresponding bromoalkane for $C_{n\text{-}s\text{-}n}$, and (3-bromopropyl)trimethylammonium bromide with *N,N,N*-alkyldimethylamine or bromohexadecane with a corresponding amine for $C_{n\text{-}s\text{-}1}$. For the details of the method, see (*22*).
10. The normalized adsorption α_s is obtained from the isotherm on a reference sample and is plotted against relative pressure P/P_0 to obtain a standard α_s curve. The α_s curve can then be used to construct an α_s plot from the isotherm of a test sample. [For details, see S. J. Gregg and K. S. W. Sing, *Adsorption, Surface Area and Porosity* (Academic Press, London, 1982)].
11. A common synthesis procedure was applied in our experiments: The surfactant was first dissolved in a basic solution (such as NaOH) or an acidic solution (such as HCl), and then TEOS or another silicate source was added. The resulting mixture was stirred at room temperature for a certain time, and then heated if a high reaction temperature was desired. The solid product was recovered by filtration and dried at room temperature.
12. This structure was identified as belonging to the space group $P6_3/mmc$. This assignment was made by x-ray diffraction and by studies of transmission electron microscopy. The absence of certain types of *hkl* reflections along with the presence of a symmetry center and the finding of a hcp structure (based on the *a/c* ratio and the analogy of typical hcp structures) were used in this identification. Further details of the crystallographic analysis will be discussed elsewhere (R. Leon, Q. Huo, P. Petroff, G. D. Stucky, in preparation).
13. D. Schiferl *et al.*, *Acta Crystallogr. C* **39**, 1151 (1983).
14. D. T. Cromer, R. L. Mills, D. Schiferl, L. A. Schwalbe, *Acta Crystallogr. B* **37**, 8 (1981).
15. K. Fontell, K. K. Fox, E. Hansson, *Mol. Cryst. Liq. Cryst.* **1**, 9 (1985).
16. H. Hagslatt, O. Soderman, B. Jonsson, *Langmuir* **10**, 2177 (1994).
17. R. DeLisi and S. Milioto, *Chem. Soc. Rev.* **23**, 67 (1994).
18. M. J. Rosen, *Surfactants and Interfacial Phenomena* (Wiley-Interscience, New York, 1989).
19. K. S. W. Sing *et al.*, *Pure Appl. Chem.* **57**, 603 (1985).
20. P. J. Branton *et al.*, *Faraday Trans.* **90**, 2965 (1994).
21. M. R. Bhambhani, P. A. Cutting, K. S. W. Sing, D. H. Turk, *J. Colloid Interface Sci.* **38**, 109 (1972).
22. R. Zana *et al.*, *Langmuir* **7**, 1072 (1991).
23. E. Alami, H. Levy, R. Zana, *ibid.* **9**, 940 (1993).
24. R. Zana and Y. Talmon, *Nature* **362**, 228 (1993).
25. In order for one to directly synthesize the bicontinuous cubic ($Ia\bar{3}d$) phase, the presence of MCM-48 (from use of cetyltrimethylammonium as the template), ethanol (which comes from the silica source TEOS), or a polar organic additive [such as $(CH_3)_2NCH_2CH_2OH$, $N(CH_2CH_2OH)_3$] with fumed silica (Cab-o-Sil) as the silica source is necessary [for details, see (*1*–*3*)].
26. Funds were provided by the Office of Naval Research (G.D.S. and Q.H.), NSF grant DMR 92-08511 (G.D.S. and Q.H.), Air Products (G.D.S. and Q.H.), Mobil (G.D.S.), and the NSF Science and Technology Center for Quantized Electronic Structures (QUEST) [grant DMR-91-20007 (R.L. and P.M.F.)]. This work made use of the Materials Research Laboratory Central Facilities supported by NSF award DMR-9123048.

29 November 1994; accepted 8 March 1995

Solar-Like M-Class X-ray Flares on Proxima Centauri Observed by the ASCA Satellite

Bernhard Haisch, A. Antunes, J. H. M. M. Schmitt

Because of instrumental sensitivity limits and stellar distances, the types of x-ray flares observable on stars have been intrinsically much more energetic than those on the sun. Such enormous events are a useful extrapolation of the solar phenomenon if the underlying assumption is correct that they form a continuous sequence involving similar physical processes as on the sun. The Advanced Satellite for Cosmology and Astrophysics (ASCA), with its greater sensitivity and high-energy response, is now able to test this hypothesis. Direct comparison with solar flares measured by the x-ray–monitoring Geostationary Operational Environmental Satellites (GOES) is possible. The detection of flares on Proxima Centauri that correspond to GOES M-class events on the sun are reported.

Geomagnetic storms associated with the largest solar flares can cause communications disruptions and even power outages. For example, the event associated with the X-class flare of 10 March 1989 blacked out the Hydro-Quebec power system (*1*). Non-negligible radiation exposure of passengers on long commercial flights can result during major events, especially in the auroral latitude zones. Understanding solar flares is therefore of some importance, and the monitoring of solar activity and the development of flare forecasting ability have been long-standing programs in both the U.S. Department of Commerce and Department of Defense (*2*). Since 1969, the key observational component in this system has been the GOES series of the National Oceanic and Atmospheric Agency (NOAA), which continuously monitor the solar x-ray flux.

Stellar flares have been observed for 20 years to emit x-rays, but the events must be much larger—by as much as a factor of 10^4—than even the most energetic on the sun in order to be detected across the enormous distances. While stellar "superflares" are of considerable interest, it is equally important to ascertain whether and with what frequency commonplace solar-like events occur on stars. Being able to observe such events is an important test of the working hypothesis that we are dealing with scaled-up versions of the same physical phenomenon. The Japanese ASCA satellite (*3*) has now succeeded in such a detection, observing very typical M-class solar-like flares on the next nearest star, Proxima Centauri.

The GOES classification for solar x-ray flares is a linear function of the flux in the ~1 to 8 Å band by which criterion flares are assigned a class of C, M, or X. The satellite also measures a harder spectral component (~0.5 to 4 Å) in which the flux is typically 10 to 100 times weaker. This weakness is a result of the steeply falling thermal emissivity of plasma at flaring temperatures $T > 10^7$ K for wavelengths $\lambda < 2$ Å (Fig. 1). The plotted spectrum is a simulation based on the plasma emissivity model of Mewe *et al.* (*4*) applied to a flare differential emission measure, which represents the amount of radiating material at the distribution of temperatures typical for flares (*5*, *6*). For this spectral distribution, the GOES band measures 63% of the actual flux in an ideal 1 to 8 Å band because the

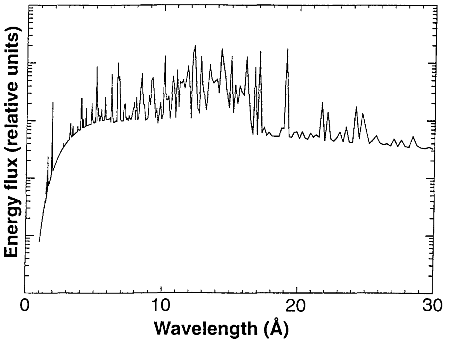

Fig. 1. Spectrum synthesized with the use of a solar flare differential emission measure and a plasma emission code accounting for both lines and continuum radiation in the 1 to 30 Å region.

B. Haisch, Lockheed Solar and Astrophysics Laboratory, Division 91-30, Building 252, 3251 Hanover Street, Palo Alto, CA 94304, USA.
A. Antunes, Institute of Space and Astronautical Sciences, 3-1-1 Yoshinodai, 229 Sagamihara-shi, Kanagawa, Japan.
J. H. M. M. Schmitt, Max-Planck-Institut für Extraterrestrische Physik, D-85740 Garching, Germany.